Research Article | Vol. 28, No. 8 / 13 April 2020 / Optics Express 11451
Optics EXPRESS

Design of a six-gas NDIR gas sensor using an integrated optical gas chamber

HEHUAN LIU, YUNBO SHI,* AND TIAN WANG

The Higher Educational Key Laboratory for Measuring & Control Technology and Instrumentations of Heilongjiang Province, School of Measurement-Control Technology & Communications Engineering, Harbin University of Science and Technology, Harbin 150080, China
*shiyunbo@hrbust.edu.cn

Abstract: A non-dispersive infrared (NDIR) gas sensor with an integrated optical gas chamber was designed to accurately detect multiple gas concentrations in a complex polluted environment. This chamber consists of a hexagonal prism shell and a reflection plate. In particular, six dual-channel infrared detectors for sensing different gases and one collimated infrared light source are integrated in the gas chamber. The IR light emitted by the collimated IR light source arrives at these detectors after four reflections. The result of simulation and data collection for optical path length and luminous flux shows that the average optical path length in the chamber is 63 mm, and the effective utilization rate of the luminous flux can reach 78.8%. The highly compact NDIR sensor can detect the concentrations of a mixture of gases (CO, CO_2, CH_4, H_2CO, NH_3, and NO with a volume fraction ranging from 0 to 4%).

1. Introduction

Gas pollution in all environments and from many sources leads to intermixing of both poisonous and deleterious species, which have harmful effects on our health [1–3]. Optical gas sensors have better selectivity and lesser toxicity than contact sensors such as a semiconductor gas sensor [4,5]. One such optical gas sensor, the non-dispersive infrared (NDIR) gas sensor, offers both small volume and strong practicality making it suitable to detect gases with asymmetric molecular structures [6–12]. Gases with asymmetric structures have different infrared absorption peaks, according to Lambert's law, [Eq. (1)]:

$$I = I_0 \cdot e^{-KCL}, \tag{1}$$

Where I_0 represents the intensity of infrared light incident; I represents the intensity of infrared light emitted; K represents the correlation coefficient of gas absorption; L represents the effective optical path length for infrared light absorption; and C represents the gas concentration for absorbing infrared light.

The NDIR gas sensor can detect the absorption of infrared light at specific wavelengths, and the concentration of the corresponding gas can be measured. It primarily comprises an infrared light source, an optical gas chamber, and a detector [13]. The infrared light emitted by the light source is projected onto the infrared detector along the set optical path. The target gas enters the optical gas chamber through the air hole and in the chamber absorbs the infrared light [14–16]. The detector uses the infrared light intensity before and after gas absorption, and the concentration is calculated through Lambert's law, [Eq. (1)].

The role of the optical gas chamber includes:

- ensuring that the emitted IR light reaches the detector unaffected,
- building an appropriate absorption light path for the target gas, and
- offering a robust and practical structure.

#388713 https://doi.org/10.1364/OE.388713
Journal © 2020 Received 21 Jan 2020; revised 27 Mar 2020; accepted 28 Mar 2020; published 2 Apr 2020

Optics EXPRESS

Gas detection in different environments can be realized by designing the optical gas chamber and installing the infrared light source and detector with a suitable size. Researchers often use optical software to simulate and emulate light paths and fluxes [17–19].

D. S. Shah designed a cylindrical optical air chamber with a length of 25 mm and a diameter of 20 mm and analyzed the light in the air chamber with Zemax software [20]. J. Park designed a unique optical cavity structure with double concave mirrors. The light simulation results show that the light emitted by the infrared light source is reflected twice and projected on the optical detector in a converging state. The light path length in the optical air chamber is 65 mm. The volume of the optical gas chamber is 4.5 cm^3 [21,22]. In the optical gas chamber designed by J. Hodgkinson, a composite parabolic collector is used. The detector and light source are enclosed in an optical gas chamber in the above-mentioned way. Zemax shows that the infrared light emitted by the infrared light source is reflected twice and then projected onto the detector, and the average effective length of the optical path is 32 mm [23]. In the optical gas chamber designed by Sieber, the average optical path length is 60 mm, and the IR source is emitted after three times of reflection, the infrared light is projected on the thermopile element [24]. Several optical gas sensors are used outdoors for single gas detection. Tan's optical gas chamber with an ellipsoid surface used an IR projection on four infrared detectors after three reflections. The optical path length is 26 mm, allowing the measurement of three gases in a small volume optical gas chamber [25], it is a small cylinder with a diameter of 20 mm and a height of 20 mm. Among the commercial sensors, MH-Z14 and MH-Z19 NDIR gas sensors are widely used. The optical gas chamber of MH-Z14 is navicular with a size of 57.5 × 31.5 × 14.6 mm, and the optical gas chamber of MH-Z19 is rectangular with a size of 26.5 × 20.5 × 8.5 mm. Both sensors are used to detect single gas.

Compared to other optical gas sensor types, the prominent advantage of NDIR gas sensor is its small size and portability. The optical gas chamber in the small-sized NDIR gas sensor also requires a long optical path and multi-gas detection, thereby limiting the development of NDIR gas sensors for complex gas environments. We designed an NDIR gas sensor for six gas species. The design included a collimated infrared light source, a multi-reflective small volume optical air chamber, and six dual-channel infrared detectors. By setting the size and angle of the reflective plate in the optical gas chamber, a reflective infrared light path was constructed. Simulation and data collection for infrared light path length and luminous flux showed an average infrared light path length in the chamber of 63 mm, and an effective utilization rate of the luminous flux at 78.8%. The so-designed small NDIR can detect the concentration of a mixed gas that may contain CO, CO_2, CH_4, H_2CO, NH_3, and NO at volume fractions ranging from 0 to 4%. Its size allows portability to accurately measure gas concentrations in complex environments, making it fit for applications in production, living environments, and other scenarios where such species may occur.

2. Sensor design

2.1. Light source

The IR light source is one of the components of the NDIR gas sensor. Two types are typically used in NDIR gas sensors, either the collimated or divergent style. A collimated infrared light source consists of an emitting chip and a collecting and reflecting cup, such as EMIRS200. The collection of the IR light can more accurately project the collimated light onto the detector. The wavelength coverage ranges from 2 µm to 14 µm, enabling broad gas detection. The divergent infrared light source stems from IR lamp beads, such as IR715EN. The infrared light emitted by the lamp beads is stray light and cannot be directed onto the detector. The IR light emitted by the filament is confined within 5 µm by the lamp glass. The comparison of the two infrared light sources is shown in Fig. 1.

Optics EXPRESS

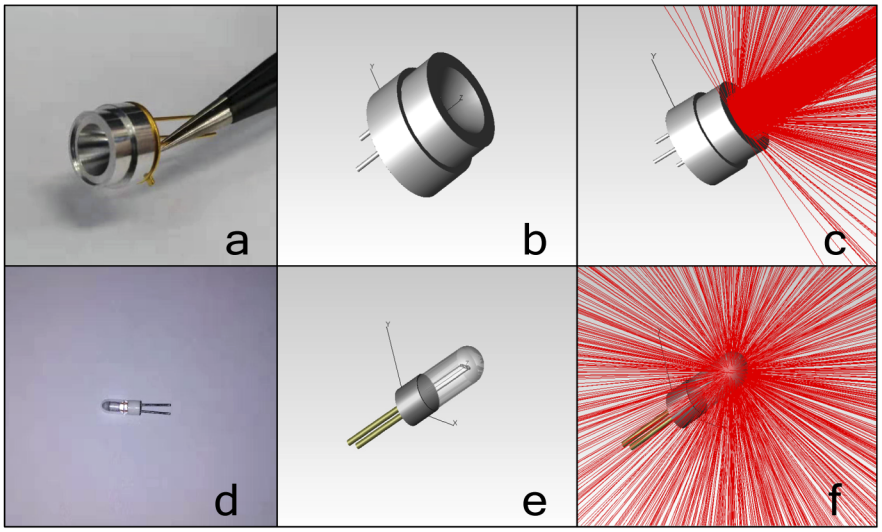

Fig. 1. (a) EMIRS200; (b) close-up sketch; (c) emission in operation; (d) IR715EN; (e) close-up sketch; (f) emission in operation.

Most of the rays from a collimated IR light source are parallel, with only a small portion scattered, while the divergent IR light source predominantly scatters. Our design required projection along the prescribed path; hence, a collimated IR light source was selected. The selected EMIRS200 light source is an electrically modulated light source with blackbody radiation characteristics. Its optical power increases with an increase of working temperature.

2.2. Optical gas chamber

The optical path can be effectively extended by adding reflecting surfaces in the optical gas chamber. We designed a hexagonal prism-shaped chamber to do just that. Hexagonal pyramid-shaped reflecting plates and a partition plate parallel to the chamber walls were built into the interior. These parts constituted the three infrared light-reflecting surfaces: top reflecting surface, built-in partition reflecting surface and chamber shell reflecting surface. Figure 2 reveals the cross-section of the optical gas chamber and its dimensions. The IR light source is located at the center of the bottom plate. After the reflected infrared light is reflected by the top reflection plate, it enters the parallel reflection area formed by the shell and the built-in partition for three reflections, and finally is projected on the receiving surface of the infrared detector. A total of four reflections were successfully performed in the set route to achieve optical path extension.

In the design, six vent holes are provided on the top plate of the optical gas chamber and the top reflection plate. Silica gel desiccant was added between the top plate of the optical chamber and the top reflecting plate to completely remove water molecules that would impede on accuracy with interfering infrared absorption peaks. The light-reflecting surface was coated with copper to improve the utilization rate of infrared light in the chamber. The reflectivity of copper in the range of 2 µm ~ 5 µm is 96% ~ 98%. Thus, there will be a small loss of light when reflected in the optical gas chamber. In the process of simulating the optical path, the material parameters of the reflecting surface were modified to make the simulation results to be closer to reality. Combined with the above requirements and the manufacturing process of the optical chamber, the chamber was divided into three parts for manufacturing and assembly: top plate, air chamber shell and reflector. Figure 3 shows a static diagram of its fabrication and assembly. With this

Optics EXPRESS

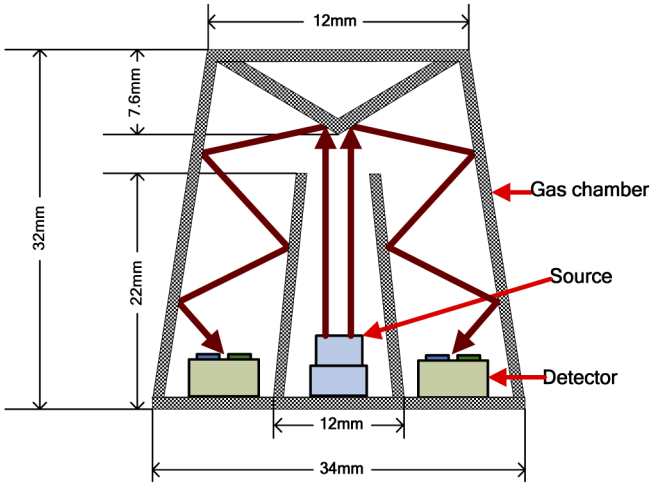

Fig. 2. Sectional view of optical gas chamber.

method, the internal components of the optical chamber can reflect light comprehensively and the design is also convenient for the filling of silica gel desiccant.

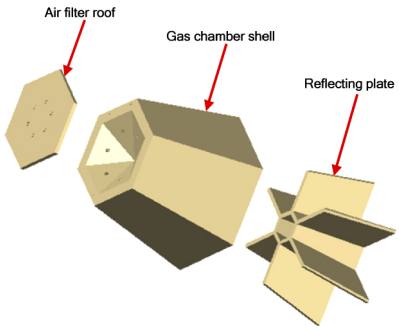

Fig. 3. Assembly of the optical gas chamber.

The light source and detector are horizontally arranged on the PCB detection base plate. The IR light source is located at the center of the plate and the detector between the inner partition and the outer shell (60° to each other). The optical air chamber is buckled on the PCB bottom plate from top to bottom during assembly, and sealed. The assembly diagram of gas chamber and base plate is shown in Fig. 4:

2.3. Detector

A dual-channel pyroelectric infrared detector is used to detect the infrared light intensity before and after gas absorption. The pyroelectric material releases current when heated. The current signal is then converted into voltage signal output through the pre-amplification terminal. The detection channel and the reference channel are equipped with covered compensation elements. The compensation element outputs the opposite signal to the detector element when the ambient temperature changes and the detector produce a mechanical vibration, which will compensate for the impact of environmental temperature change and mechanical vibration. In addition, the infrared light variation caused by optical jitter will have the same effect on the two channels on the same detection surface. In this respect, the reference channel compensates the error caused by

Optics EXPRESS

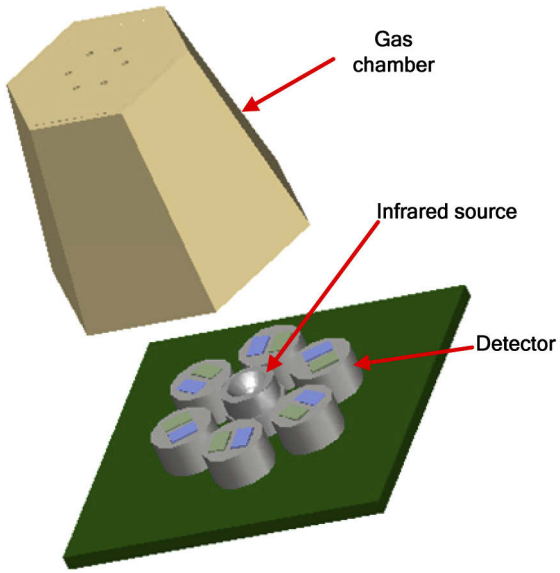

Fig. 4. Assembly of optical air chamber and base plate.

optical jitter. As shown in Fig. 5, the difference between the detection channel and the reference channel is that a band-pass filter of different wavelengths is installed above the detection chip, and the detection channel filter can detect the infrared light intensity I_1 after gas absorption through the infrared light at the wavelength of the main absorption peak of the target gas, while the infrared light passing through the reference channel filter is not absorbed by the detection gas, and the initial infrared light intensity I_0 is detected. After the preamplifier circuit amplifies, the reference channel output voltage is U_0 [Eq. (2)] and the detection channel output voltage is U_1 [Eq. (3)].

According to Lambert's law:

$$U_0 = S_0 I_0, \tag{2}$$

$$U_1 = S_1 I_0 e^{-KCL}, \tag{3}$$

Here, S_0 and S_1 are system-related constants; K is the correlation coefficient of gas absorption, which is related to the absorption property of the target gas and the filter selected; and L is the length of the optical path. In the determined infrared gas detection system, the above coefficients are constants. By dividing the above two formulae, the influence of light intensity in concentration calculation can be eliminated, and the relationship between gas concentration and output voltage of a dual channel pyroelectric detector can thus be obtained [Eq. (4)]:

$$C = -\frac{1}{KL} \ln \frac{U_1}{U_0} - \frac{1}{KL} \ln \frac{S_1}{S_0}. \tag{4}$$

When using the dual-channel infrared detector to verify the effectiveness of the designed optical chamber. The parameter *Fa* (fractional absorbance) is introduced to record the relative voltage change when the gas concentration changes [Eq. (5)]:

$$Fa = \frac{U_0 - U_1}{U_0} = 1 - e^{-KCL}. \tag{5}$$

The detection of different gases can be realized by installing filters with different wavelengths on the detection channel based on the IR absorption peaks. The optical gas chamber in this

Optics EXPRESS

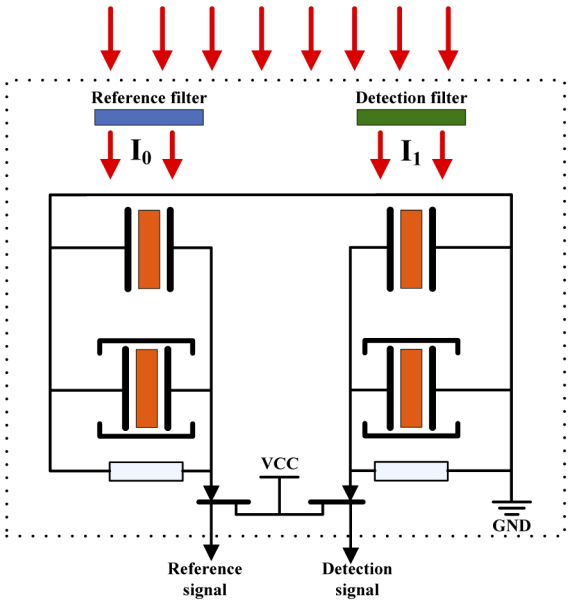

Fig. 5. Schematic of dual-channel detector.

design can accommodate six dual-channel infrared detectors at the same time; therefore, it can detect six different gases. If the main infrared absorption peaks of the target gas overlap, the detection error will occur due to the cross absorption. After searching different gas absorption peaks through HITRAN database [26], CO, CO_2, CH_4, H_2CO, NH_3, and NO are finally selected as detection targets. The main infrared absorption peaks of the above six gases do not overlap. Filters are used to avoid cross interference caused by overlapping of edge absorption peaks. A filter that only passes through a wavelength that can be absorbed by a single gas is a suitable filter. Moreover, adding water vapor filter material at the sensor air hole can eliminate the interference of water vapor increasing detection accuracy. The dual-channel infrared detector used in the design detects different gases by installing filters of different wavelengths. Parameters of target gas and corresponding filter are shown in Table 1. The gas parameters include absorption peak and molar absorption coefficient (KNa). The infrared light intensity of gas absorption is related to the absorption coefficient K, which is mainly determined by the molar absorption coefficient of the gas itself, according to Lambert's law. The center wavelength (CWL) and half power bandwidth (HPB) are two important parameters for choosing the filter.

Table 1. Parameters of target gases and corresponding filters

Target Gas	Absorption peak	KNa at peak	Filter CWL	Filter HPB
CO	4.66 μm	5.4×10^{1}	4.64 μm	180 nm
CO_2	4.26 μm	2.8×10^{2}	4.26 μm	180 nm
CH_4	3.31 μm	4.3×10^{1}	3.20 μm	30 nm
H_2CO	3.56 μm	6.5×10^{0}	3.65 μm	125 nm
NH_3	10.30 μm	1.7×10^{1}	10.20 μm	220 nm
NO	5.30 μm	1.5×10^{1}	5.25 μm	90 nm
REF	3.90 μm		3.90 μm	180 nm

Optics EXPRESS

The six dual-channel infrared detectors in this design have twelve output signals which are processed in the form of a transfer board. The IR light source is in the center of the plate, and the detector is located between the gas chamber shell and the reflection baffle plate. The adapter plate integrated detectors and IR light source is shown in Fig. 6.

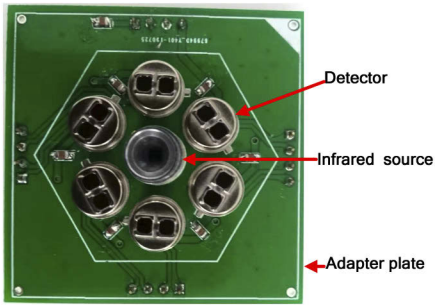

Fig. 6. The adapter plate integrated detectors and IR light source.

3. Simulation of the optical gas chamber

3.1. Optical path

The optical chamber needs to establish the optical path length to project the IR light on the detector entirely. The optical path simulation of the designed optical chamber was carried out by TracePro software in this study. The IR light source was set as the ideal collimated light, and the optical chamber was set as translucent to visually observe the reflection path of infrared light in the designed optical chamber. From the side-up view, the six infrared lights projection path can be clearly recorded, and the single path of infrared light projection path can also be observed from the side view. The light simulation under two different angles is shown in Fig. 7.

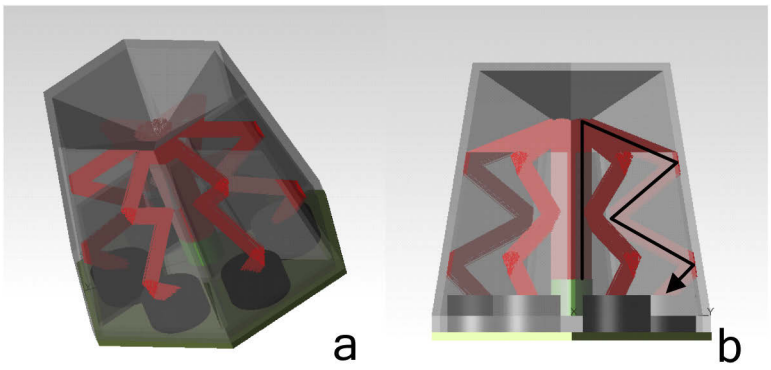

Fig. 7. Optical path of ideal parallel infrared light source: (a) side-up angle; (b) side angle.

By observing the light path under the condition of setting ideal parallel light, the infrared light is reflected four times between the air chamber shell and the reflection plate and is finally directed the detector, consistent with the designed optical path. In practical applications, collimating the light depends on the reflecting cup. The reflecting cup can collimate and gather most of the small amount of scattered light.

Real situations can be predicted by replacing the ideal collimated light source with a collimated light source and performed light simulation on the designed NDIR gas chamber, as was done in

Optics EXPRESS

this study. The six infrared lights projection path can be clearly recorded, and the single path of the infrared light projection path can be observed from the side. The simulation was conducted under two different angles (Fig. 8). In actual applications, the collimated light source cannot completely emit the ideal parallel light. Compared with the simulation result of the optical path using the ideal parallel light source, there is a small amount of stray light reflection in the optical gas chamber, but most of the light is still projected along the ideal parallel light path onto the detector.

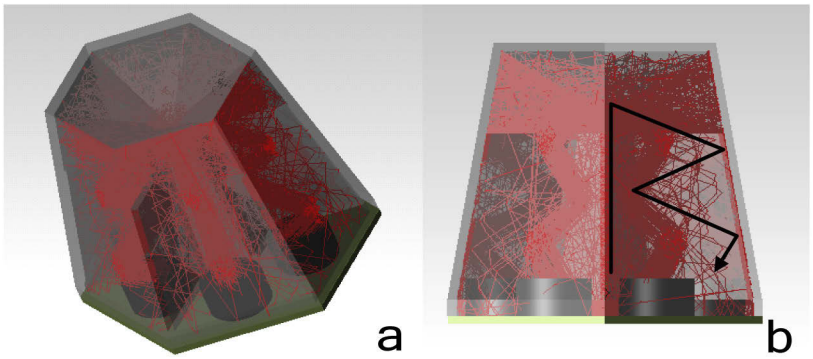

Fig. 8. Optical path of ideal parallel infrared light source: (a) side-up angle; (b) side angle.

In the NDIR gas sensor, an appropriate optical path length can ensures that the target gas fully absorbs the infrared light. We analyzed the optical path length of the infrared light projected on each infrared detector. The analysis result is shown in Fig. 9.

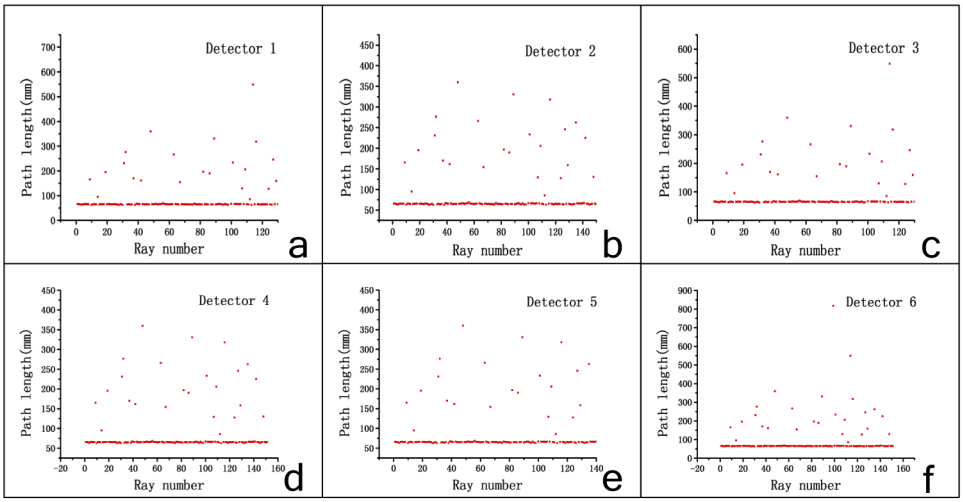

Fig. 9. Collection of optical path lengths.

Most of the collimated light was emitted as parallel light; only a small part is stray light. The stray light cannot follow the set optical path reflection in the designed optical gas chamber and will be projected onto the detection floor and the detector after multiple un-directional reflections in the chamber. Most of the light was projected to the receiving surface of the detector along the preset light ray track, except for the stray light projection points after multiple reflections. The average length was 63 mm.

Optics EXPRESS

3.2. Detector luminous flux

The surface of the six-channel infrared detector is an infrared light receiver. This study collected the light flux for comparison. According to the actual parameters of the infrared light source, the output optical power of the infrared light source was set to 39 mW, the surface of the optical gas chamber was set to a copper reflection state, and the output light quantity was set to 1000. The collected detector luminous flux is shown in Fig. 10.

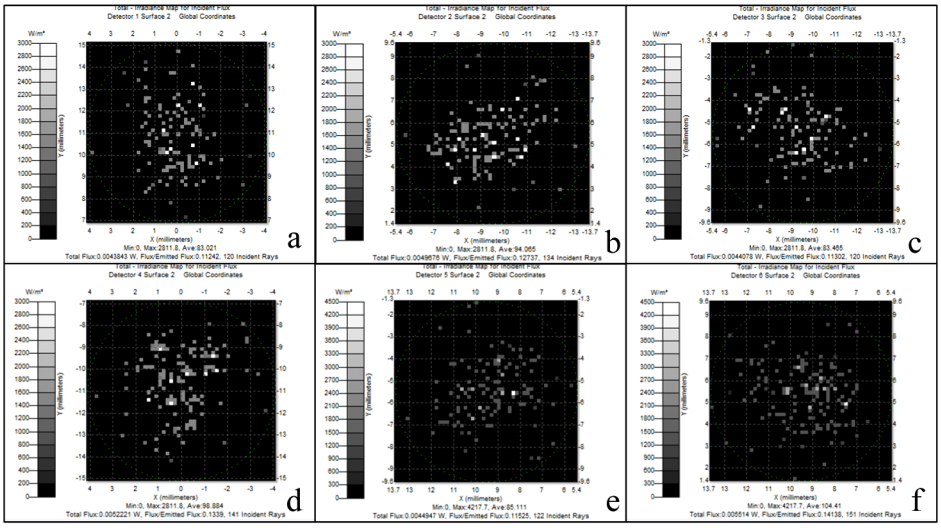

Fig. 10. Detector Luminous Flux Collection: (a) Detector No. 1; (b) Detector No. 2 ; (c) Detector No. 3; (d) Detector No. 4; (5) Detector No. 5; (6) Detector No. 6.

The number of projected rays and light power received by the six independent light-receiving surfaces of the detectors are relatively uniform. The effective utilization rate of the infrared light from the light source can reach 78.79% when adding up all light passing through all the effective receiving surfaces.

4. Experimental results and discussions

A square shell was installed outside the optical gas chamber, and the adapter plate was completely attached to the chamber to connect and seal the adapter plate with the optical gas chamber. Such a structure can largely improve the pressure resistance of the optical gas chamber. After the square shell has been installed, the overall volume of the chamber was only $4.8 \times 4.8 \times 3.2$ cm. The designed NDIR gas sensor is shown in Fig. 11.

The test process of the designed gas sensor is shown in Fig. 12.

The mixed gas with species in different volume fractions was passed into a nitrogen environment test box for testing to test the air chamber. The test signal data of different gases passing through the same amplification circuit are different, because the absorption coefficients of the six gases in the selected wavelength range are different by orders magnitude. The measured data was divided into three groups according to the order of the molar absorption coefficients of the corresponding gases (as shown in Fig. 13).

The test range of the six gases was 0–4% (volume fraction), and the test gradient was 0.5% (volume fraction). The results showed that the designed NDIR gas sensor had a linear response to the mixed gases of different concentrations. The concentration of the six gases could be successfully detected with this designed optical gas chamber. According to the actual measurement results, the detection parameters of the sensor are shown in Table 2.

Optics EXPRESS

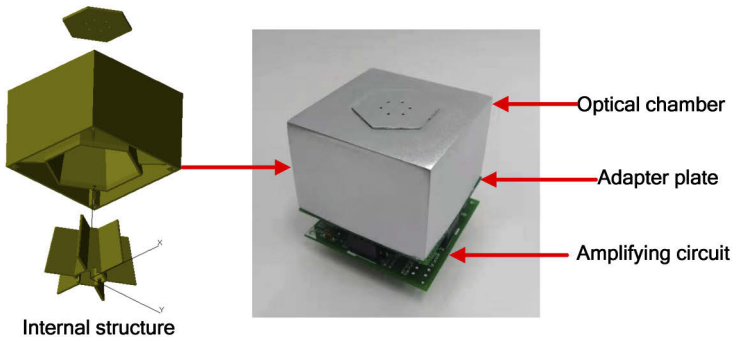

Fig. 11. Designed NDIR gas sensor.

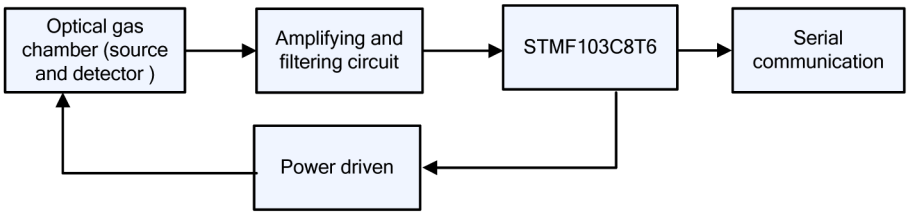

Fig. 12. Signal processing flowchart.

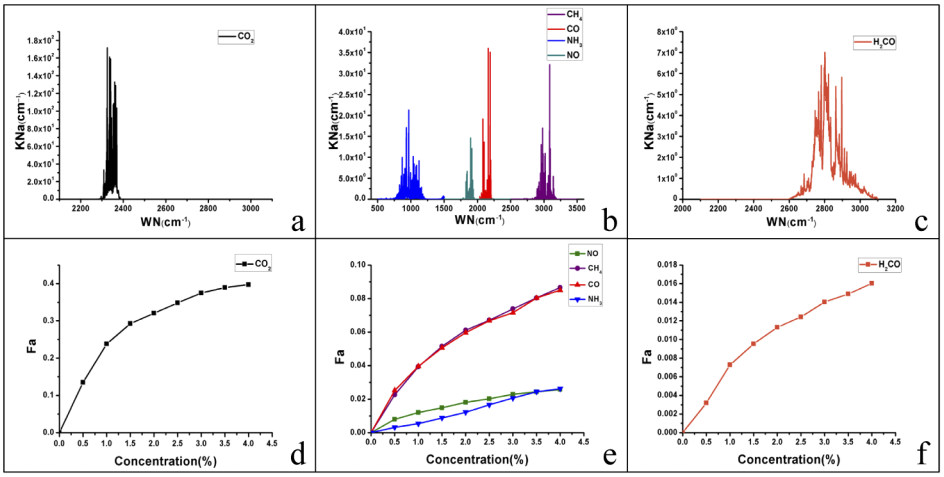

Fig. 13. (a), (b), (c): Absorption peak and related absorption coefficients of CO_2, CH_4, CO, NH_3, NO, and H_2CO; (d), (e), (f): Test results of CO_2, CO, CH_4, NH_3, NO, and H_2CO.

Table 2. Detection parameters of the sensor

Gas	Detection limit	Accuracy	Precision
CO_2	100ppm	±0.01%	0.021
CO	500ppm	±0.05%	0.022
CH_4	500ppm	±0.05%	0.035
NH_3	5000ppm	±0.5%	0.031
NO	5000ppm	±0.5%	0.052
H_2CO	5000ppm	±0.5%	0.039

Optics EXPRESS

The simulation and experiment results show that the optical gas chamber in this study can detect six kinds of gases. Moreover, in this small optical gas chamber, the light can be reflected four times, which can extend effectively and project to the receiving surface of the detector accurately. Compared with existing NDIR gas sensors, this sensor has a small volume, can detect multiple gases, and has a long optical path. The new idea is extended for the design of optical gas chamber in the NDIR gas sensor.

5. Conclusion

This study proposes a high-performance gas sensor based on the NDIR detection principle to effectively and accurately detect the concentrations of six gases (CO, CO_2, CH_4, H_2CO, NH_3, and NO) simultaneously. A highly integrated gas chamber, comprising a hexagonal prism shell and a reflection plate, with advantages such as small size, high luminous flux utilization rate, and long optical path, was developed and incorporated into the NDIR gas sensor. This type of sensor can be applied for the detection of gas concentrations in environments where different gases are intermixed, e.g., in the field of urban and rural pollution monitoring. Although an optimized data processing strategy can be applied to include more types of target gases, the method proposed in this paper provides a novel model for multi-gas detection.

Funding

National Defense Basic Scientific Research Program of China (JCKY2017412C003).

Acknowledgments

The authors wish to thank the editor and reviewers for their valuable suggestions.

Disclosures

The authors declare no conflicts of interest.

References

1. D. D. Lee and D. Lee, "Environmental gas sensors," IEEE Sens. J. **1**(3), 214–224 (2001).
2. C. R. Martin, N. Zeng, A. Karion, R. R. Dickerson, X. Ren, B. N. Turpie, and K. J. Weber, "Evaluation and environmental correction of ambient CO_2 measurements from a low-cost NDIR sensor," Atmos. Meas. Tech. **10**(7), 2383–2395 (2017).
3. J. de Castro, J. Meneses, S. Briz, and F. López, "Nondispersive infrared monitoring of NO emissions in exhaust gases of vehicles," Rev. Sci. Instrum. **70**(7), 3156–3159 (1999).
4. I. Cacciari and G. C. Righini, *Solid State Gas Sensing* (Springer, 2009), chap. 6.
5. J. Hodgkinson and R. P. Tatam, "Optical gas sensing: a review," Meas. Sci. Technol. **24**(1), 012004 (2013).
6. R. Frodl and T. Tille, "A High-Precision NDIR CO_2 Gas Sensor for Automotive Applications," IEEE Sens. J. **6**(6), 1697–1705 (2006).
7. D. Gutmacher, U. Hoefer, and J. Wöllenstein, "Gas sensor technologies for fire detection," Sens. Actuators, B **175**, 40–45 (2012).
8. J. Antón and M. Silva-López, "Optical cavity for auto-referenced gas detection," Opt. Express **19**(27), 26079–26087 (2011).
9. Z. Zhu, Y. Xu, and B. Jiang, "A One ppm NDIR Methane Gas Sensor with Single Frequency Filter Denoising Algorithm," Sensors **12**(9), 12729–12740 (2012).
10. L. B. Mendes, N. W. Ogink, N. Edouard, H. J. van Dooren, F. Tinoco Ide, and J. Mosquera, "NDIR Gas Sensor for Spatial Monitoring of Carbon Dioxide Concentrations in Naturally Ventilated Livestock Buildings," Sensors **15**(5), 11239–11257 (2015).
11. H. Wang, J. Wang, X. Ma, W. Chen, D. Chen, and Q. Li, "Note: A NDIR instrument for multicomponent gas detection using the galvanometer modulation," Rev. Sci. Instrum. **88**(11), 116103 (2017).
12. J. Mayrwöger, W. Reichl, and B. Jakoby, "Design of an NDIR gas sensor with two non-symmetric Fabry-Perot absorber-structures working as IR-emitter and IR-detector," Proc. SPIE **7726**, 77260J (2010).
13. A. Rogalski, "Infrared detectors: an overview," Infrared Phys. Technol. **43**(3-5), 187–210 (2002).
14. J. Hodgkinson, R. Smith, W. Ho, J. R. Saffell, and R. P. Tatam, "A low cost, optically efficient carbon dioxide sensor based on nondispersive infra-red (NDIR) measurement at 4.2μm," Proc. SPIE **8439**, 843919 (2012).

Optics EXPRESS

15. Q. Tan, W. Zhang, C. Xue, J. Xiong, Y. Ma, and F. Wen, "Design of mini-multi-gas monitoring system based on IR absorption," Opt. Laser Technol. **40**(5), 703–710 (2008).
16. J. Kim, K. Lee, and S. Yi, "NDIR Ethanol Gas Sensor with Two Elliptical Optical Structures," Procedia Eng. **168**, 359–362 (2016).
17. G. Zhang, Y. Li, and Q. Li, "A miniaturized carbon dioxide gas sensor based on infrared absorption," Opt. Laser. Eng **48**(12), 1206–1212 (2010).
18. C. Chen, Y. Zhang, Y. He, K. Yan, and Y. Gao, "Simulation Method for Optical System of an Infrared Gas Sensor," in *Proceedings of Eighth International Conference on Measuring Technology and Mechatronics Automation* (IEEE, 2016), pp. 597–600.
19. T. Liang, X. J. Yang, C. Y. Xue, and W. D. Zhang, "Study of Optical Gas Chamber Based on Infrared Gas Sensor," Adv. Mater. Res. (Durnten-Zurich, Switz.) **472-475**, 1102–1106 (2012).
20. D. S. Shah, M. Fuke, S. Upadhyay, A. Verma, and S. U. Rehman, "Development and characterization of NDIR-based CO_2 sensor for manned space missions," *Society of Photo-optical Instrumentation Engineers. SPIE Conference Series*, (2016).
21. J. Park, H. Cho, and S. Yi, "NDIR CO_2 gas sensor with improved temperature compensation," Procedia Eng. **5**, 303–306 (2010).
22. J. Park and S. Yi, "Temperature compensated NDIR CH_4 gas sensor with focused beam structure," Procedia Eng. **5**, 1248–1251 (2010).
23. J. Hodgkinson, R. Smith, W. O. Ho, J. R. Saffell, and R. P. Tatam, "Non-dispersive infra-red (NDIR) measurement of carbon dioxide at 4.2μm in a compact and optically efficient sensor," Sens. Actuators, B **186**, 580–588 (2013).
24. I. Sieber, H. Eggert, K. Suphan, and O. Nüssen, "Optical modeling of the analytical chamber of an IR gas sensor," Proc. SPIE **4408**, 272–282 (2001).
25. Q. Tan, L. Tang, M. Yang, C. Xue, W. Zhang, J. Liu, and J. Xiong, "Three-gas detection system with IR optical sensor based on NDIR technology," Opt. Laser. Eng **74**, 103–108 (2015).
26. E. Gordon, L. S. Rothman, C. Hill, R. V. Kochanov, Y. Tan, P. F. Bernath, M. Birk, V. Boudon, A. Campargue, K. V. Chance, B. J. Drouin, J. M. Flaud, R. R. Gamache, J. T. Hodges, D. Jacquemart, V. I. Perevalov, A. Perrin, K. P. Shine, M. A. H. Smith, J. Tennyson, G. C. Toon, H. Tran, V. G. Tyuterev, A. Barbe, A. G. Császár, V. M. Devi, T. Furtenbacher, J. J. Harrison, J. M. Hartmann, A. Jolly, T. J. Johnson, T. Karman, I. Kleiner, A. A. Kyuberis, J. Loos, O. M. Lyulin, S. T. Massie, S. N. Mikhailenko, N. Moazzen-Ahmadi, H. S. P. Müller, O. V. Naumenko, A. V. Nikitin, O. L. Polyansky, M. Rey, M. Rotger, S. W. Sharpe, K. Sung, E. Starikova, S. A. Tashkun, J. V. Auwera, G. Wagner, J. Wilzewski, P. Wcisło, S. Yu, and E. J. Zak, "The HITRAN2016 molecular spectroscopic database," J. Quant. Spectrosc. Radiat. Transfer **203**, 3–69 (2017).